



Molecular interaction, co-solubilization of organic pollutants and ecotoxicity of a potential carcinogenic fuel additive MTBE in water

Surajit Rakshit^a, Ranajay Saha^a, Achintya Singha^b, Zaki Shakir Abdullah Seddigi^c, Samir Kumar Pal^{a,*}

^a Department of Chemical, Biological & Macromolecular Sciences, S.N. Bose National Centre for Basic Sciences, Block JD, Sector III, Salt Lake, Kolkata 700098, India

^b Department of Physics, Bose Institute, 93/1, Acharya Prafulla Chandra Road, Kolkata 700 009, India

^c Department of Chemistry, College of Applied Sciences, Umm Al-Qura University, Makkah, 21955, Saudi Arabia

ARTICLE INFO

Article history:

Received 17 September 2012

Accepted 19 January 2013

Available online 14 February 2013

Keywords:

MTBE

MTBE aggregates in water

Physico-chemical change

Molecular interaction

Co-solubilization

Eco-cytotoxicity

ABSTRACT

We study the molecular properties and ecological consequences of a most common gasoline oxygenate, and widespread carcinogenic environmental threat, methyl *tert*-butyl ether (MTBE) upon inclusion in water. Our study shows the change of bulk properties like densities, viscosities and refractive indices of binary mixtures of water and MTBE at temperatures from 10 °C to 50 °C and over the entire composition range, under atmospheric pressure using densimetry, viscometry and refractive index measurement. The studies are clear indicative of the association of MTBE in the hydrogen bonding network and possible MTBE clustering in the aqueous solution. While, dynamic light scattering studies confirm the formation of micro-droplets (micelle-like) of MTBE in water, which still persist at 70 °C (much above the boiling point of pure MTBE, 55.2 °C), FTIR and Raman spectroscopies have distinctly unrevealed the molecular interaction of MTBE with water molecules. Co-solubilization of other potential hazardous organic matters (anthracene, naphthalene, benzo[α]pyrene and 4-(dicyanomethylene)-2-methyl-6-(*p*-dimethylamino-styryl)-4H-pyran (DCM)) in the MTBE–water mixture has also been studied. Raman spectroscopic studies confirm the micelle-like cluster of MTBE to be a potential host of the organic pollutants in the aqueous environments. The picosecond-resolved spectroscopic studies also confirm localization of DCM in the ground state, in the MTBE cluster. Our studies also show the ecotoxic effect of MTBE in model eukaryotic microorganism yeast in aqueous environments.

© 2013 Elsevier B.V. All rights reserved.

1. Introduction

The specific interaction of water molecules with hydrophobic solvents is very important from both basic science and technological application point of view. A detailed scientific understanding becomes more crucial when the hydrophobic solvent is a potential threat of environment (water in particular) and health. For example, methyl *tert*-butyl ether (MTBE) is a hydrophobic solvent; as a widely used fuel additive it is much more soluble in water (4% wt/wt) than most of the other components of gasoline. The potential risk of ground water pollution through leakage of underground storage tank of fuel containing

MTBE and unacceptable health hazards including carcinogenesis led Environmental Protection Agency (EPA) to issue an advisory on MTBE in the year 2002. Here we like to highlight that significant solubility of organic MTBE in water is also a potential threat of indirect water pollution through the enhanced co-solubilization of other sparingly soluble environmental pollutants, which has been relatively less attended in the literature. Earlier studies show that [1] the apparent water solubility of some water-insoluble organic solutes (e.g., 1,1-bis(*p*-chlorophenyl)-2,2,2-trichloroethane (DDT), 1,2,3-trichlorobenzene (TCB)) can be significantly enhanced by low concentrations of dissolved organic matter (DOM) like humic and fulvic acids. Investigation on enhanced contamination of other water pollutants in the presence of MTBE in water is one of the motives of the present study. By using picosecond resolved spectroscopy we have also explored the localization of one of the organic matters, 4-(dicyanomethylene)-2-methyl-6-(*p*-dimethylamino-styryl)-4H-pyran (DCM) and accordingly rationalized the molecular basis for the enhanced solubilization.

Due to the chemical properties like high aqueous solubility [2], low Henry's law constant [3,4], small molecular size and low volatility, MTBE is not readily amenable to treatment by conventional techniques such as air stripping and activated carbon adsorption or chemical oxidation. A significant technological advancement for the removal of the volatile MTBE from water including photo-catalytic techniques using

Abbreviations: MTBE, methyl *tert*-butyl ether; EPA, Environmental Protection Agency; DCM, 4-(Dicyanomethylene)-2-methyl-6-(*p*-dimethylamino-styryl)-4H-pyran; DDT, 1,1-Bis(*p*-chlorophenyl)-2,2,2-trichloroethane; TCB, 1,2,3-Trichlorobenzene; DOM, dissolved organic matter; FTIR, Fourier transformed infrared; DAPI, 4',6'-Diamidino-2-phenylindole; MTCC, Microbial Type Culture Collection and Gene Bank; DSC, differential scanning calorimetry; DLS, dynamic light scattering; d_H , hydrodynamic diameter; CCD, charge-coupled device; IRF, instrument response function; ρ , density; η , viscosity; n_D , refractive indices; V^E , excess molar volume; $\delta\eta$, viscosity deviations; δn_D , refractive index deviations; $\Delta_f H$, heat of fusion; x_i , mole fraction; $\Delta_{mix} H$, enthalpy of mixing.

* Corresponding author. Tel.: +91 33 2335 5708; fax: +91 33 2335 3477.

E-mail address: skpal@bose.res.in (S.K. Pal).

various nanoparticles as catalysts has been reported earlier [5–7]. However, a full-proof technique for the complete removal of MTBE from water is most desirable and yet to be developed. It has to be noted that a detailed understanding of the bulk physico-chemical properties as well as the molecular interaction of the MTBE molecules with water is important for the design of efficient removal procedure. In a recent thermodynamic study [8] on the interaction of MTBE with water, it was interestingly concluded that solubilization of MTBE in the hydrogen bond network of water is exothermic while that of the water molecules in the hydrophobic environments is endothermic. Using Fourier transformed infrared spectroscopy (FTIR) and ab initio calculation, another study has shown that C–O and C–C stretching vibrational frequencies of MTBE are heavily affected on interaction with water molecules in the diluted aqueous solution and concluded to be due to hydrogen bonding interaction of MTBE with host water molecules [9]. In spite of all those efforts, a detailed and systematic study on the water–MTBE mixture starting from bulk physico-chemical properties to molecular interaction of organic solutes in the mixture is sparse in the literature and thus is one of the motives of the present work. An ecological consequence of the MTBE contamination on the mortality of model microbial organism yeast in the aqueous environments has also been addressed.

2. Materials and methods

2.1. Chemicals

MTBE (>99.8%, anhydrous) 4',6-diamidino-2-phenylindole (DAPI) and benzo[α]pyrene were obtained from sigma/Aldrich; 4-(dicyanomethylene)-2-methyl-6-(p-dimethylamino-styryl)-4H-pyran (DCM) and coumarin 500 (C500) from Exciton. Anthracene and naphthalene were obtained from Loba Chemie. The purity of all the solvents was checked by comparing the experimental density, viscosity, refractive index and sound velocity data for pure liquids with the literature as listed in Table 1. For yeast cell culture, D-glucose (extra pure AR) and peptone from SRL and yeast extract powder from Merck were used. MTT based assay kit CCK-8, Cat. No. 96992 was obtained from Sigma. The yeast strain, *Saccharomyces cerevisiae* (Y11857) was obtained from Microbial Type Culture Collection and Gene Bank (MTCC), India. The strain was cultured at 25 °C in YPD medium (pH 7.0) comprising 0.3% yeast extract, 0.5% peptone and 1% D-glucose.

2.2. Cytotoxicity assay protocol

The MTBE induced cytotoxicity in yeast cells was assessed using the MTT based cell viability assay. Briefly, 5 ml of the cells was transferred to six different test tubes at a density of 12.5×10^6 cells ml⁻¹. The cells were then treated with various concentrations of MTBE (0.0, 7.4, 14.8, 29.6, 37.0, 44.4 mg/ml of MTBE) and incubated at 25 °C for 3 h, with shaking. The 200 μl of each of the cell suspensions was mixed with 20 μl of CCK-8 and incubated at 25 °C for 3 h, with

shaking. The absorbance of the supernatants was measured at 450 nm and from the CCK-8 standard curve the number of viable cells per ml at various known amounts of MTBE treated cell suspensions were estimated. The impact of MTBE cytotoxicity was also assessed by studying the time dependent MTT assay for the cells treated with MTBE with respect to a control experiment. Briefly in 3 ml of the yeast cell culture (in mid log phase of growth) MTBE was added at its highest solubility (44.4 mg/ml). The cells were next incubated at 25 °C with shaking in the presence of 300 μl of CCK-8. At various time intervals a specific amount of the culture was recovered and the absorbance of the supernatants was measured at 450 nm. A similar experiment was also performed for the control set.

2.3. Experimental and analytical procedures

Differential scanning calorimetry (DSC) data were obtained using a TA Instrument (DSC Q2000). Runs were carried out using a 100% N₂ purge gas flow at heating rates of 4 °C/min. During measurements, samples were positioned in alumina crucibles with a total volume of 40 μl and an internal diameter of 5 mm, with an empty sample pan and water as reference. Then, the samples were cooled to –150 °C followed by warming to 150 °C. Dynamic light scattering (DLS) measurements were done with a Nano S Malvern instrument employing a 4 mW He–Ne laser (λ = 632.8 nm) equipped with a thermostated sample chamber. All the scattered photons are collected at 173° scattering angle. The scattering intensity data are processed using the instrumental software to obtain the hydrodynamic diameter (d_H) and the size distribution of the scatterer in each sample. The instrument measures the time-dependent fluctuation in the intensity of light scattered from the particles in solution at a fixed scattering angle. Hydrodynamic diameter (d_H) of the MTBE clusters in water is estimated from the intensity autocorrelation function of the time-dependent fluctuation in intensity. d_H is defined as,

$$d_H = \frac{k_b T}{3\pi\eta D} \quad (1)$$

where k_b is the Boltzmann constant, η is the viscosity, and D is the translational diffusion coefficient. In a typical size distribution graph from the DLS measurement, the X-axis shows a distribution of size classes in nanometers, while the Y-axis shows the relative intensity of the scattered light. Density and viscosity of the mixture were measured by a density meter (model DSA5000) with an accuracy of 5×10^{-6} g cm⁻³ and automated micro viscometer (AVMn) from Anton Paar (Austria). Refractive indices of the solutions were measured by using a Rudolph J357 automatic refractometer. Fourier transform infrared spectroscopy (FTIR) experiment was carried out using a JASCO FTIR-6300 spectrometer. Each spectrum consists of 50 scans (400–1400 cm⁻¹) acquired at 0.5 cm⁻¹ resolution. Raman scattering measurements were performed in a back scattering geometry using a micro-Raman setup consisting of a spectrometer (model LabRAM HR, JobinYvon) and a Peltier-cooled

Table 1
Comparison of observed densities (ρ), viscosities (η), refractive indices (n_D) and speed of sound (u) for pure liquids with the literature values.

	Temperature/(°C)	ρ /(g · cm ⁻³)		η /(cP)		n_D		u /(m · s ⁻¹)	
		This work	Literature	This work	Literature	This work	Literature	This work	Literature
WATER	10	0.999690	0.999728 [36]	1.2927	1.3069 [37]	1.33402	1.33408 [38]	1447.15	1447.59
	20	0.998204	0.998233 [36]	1.0066	1.0020 [37]	1.33301	1.33336 [38]	1482.51	1482.66
	30	0.995653	0.995678 [36]	0.8108	0.7975 [37]	1.33154	1.33230 [38]	1509.12	1509.44
	40	0.992225	0.992247 [36]	0.6785	0.6532 [37]	1.33032	1.33095 [38]	1528.93	1529.18
	50	0.988048	0.988064 [36]	0.5833	0.5471 [37]	1.32858	1.32937 [38]	1542.72	1542.87
MTBE	10	0.752631	0.750684 [39]	0.4465	0.3920 [40]	1.37456	–	1112.75	1106.78 [39]
	20	0.742267	0.740336 [39]	0.4086	0.3861 [41]	1.36890	1.3690 [41]	1066.69	1059.43 [39]
	30	0.731722	0.729734 [39]	0.3787	0.3359 [42]	1.36385	–	1020.69	1013.37 [39]
	40	0.720962	0.718875 [39]	0.3554	–	–	–	976.24	967.07 [39]
	50	0.709949	0.707917 [39]	0.3270	–	–	–	932.23	922.21 [39]

charge-coupled device (CCD) detector. An air cooled argon ion laser with a wavelength of 488 nm was used as the excitation light source. Raman spectra of all samples have been recorded at room temperature in the frequency range of 50–4000 cm^{-1} . Steady-state absorption and emission were measured with a Shimadzu UV-2450 spectrophotometer and a JobinYvon Fluoromax-3 fluorimeter, respectively. Picosecond-resolved fluorescence transients were measured using a commercially available spectrophotometer (LifeSpec-ps) from Edinburgh Instrument, U.K. (excitation wavelength 409 nm, 80 ps instrument response function (IRF)). Fluorescence images of the yeast cell were captured with a fluorescence microscope (BX-51, Olympus America, Inc.) equipped with a 100 W mercury arc lamp and DP72 CCD camera. To show the nuclear morphology of the yeast cells before and after MTBE treatment fluorescence micrographs were taken under bright-field and stained with DAPI (4',6-diamidino-2-phenylindole) in the presence of UV excitation. The excited light was cut off by using a standard filter and the fluorescence was collected through a 100 \times objective.

3. Results and discussions

The experimental values of the densities (ρ), viscosities (η), refractive indices (n_D) and sound velocity data at 20 °C for the binary mixtures of water–MTBE at various concentrations are listed in Table 2 and are shown in Fig. 1. From the figure, it is clear that as the MTBE content increases, the density of binary mixture decreases as the density of MTBE is lower than water whereas refractive indices of the mixture increases as the refractive index of MTBE is higher than water. However, the viscosity of the binary mixtures increases with an increase in the concentration of MTBE, although the viscosity of MTBE (0.4086 $\text{mPa} \cdot \text{s}$) is lower than water (1.0066 $\text{mPa} \cdot \text{s}$). The observation can be rationalized in terms of the contraction of overall volume of the mixed solvents due to the formation of ordered hydrogen bonded structures between MTBE and water molecules. The excess molar volume (V^E), viscosity deviations ($\delta\eta$), refractive index deviations (δn_D), adiabatic compressibility (β_S) and deviation in adiabatic compressibility ($\delta\beta_S$) can be calculated from the experimental results according to the following equations [10–12], respectively,

$$V^E = (x_1 M_1 + x_2 M_2 / \rho_{\text{Mix}}) - (x_1 M_1 / \rho_1) - (x_2 M_2 / \rho_2) \quad (2)$$

$$\delta\eta = \eta_{\text{Mix}} - (x_1 \eta_1 + x_2 \eta_2) \quad (3)$$

$$\delta n_D = n_{D\text{Mix}} - (x_1 n_{D1} + x_2 n_{D2}) \quad (4)$$

$$\beta_S = 1 / \rho u^2 \quad (5)$$

$$\Delta\beta_S = \beta_{S\text{Mix}} - (x_1 \beta_{S1} + x_2 \beta_{S2}) \quad (6)$$

where x_1 and x_2 are the mole fractions; M_1 and M_2 are molar masses; ρ_1 and ρ_2 are the densities; η_1 and η_2 are the viscosities; n_{D1} and n_{D2} are the refractive indices of pure water and MTBE, and β_{S1} and β_{S2} are the adiabatic compressibility, respectively. The subscript "Mix" represents properties of the mixture. Table 2 shows that V^E values are

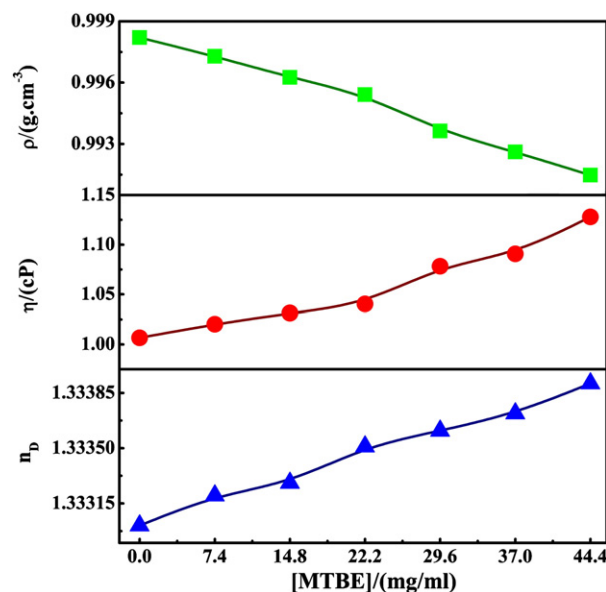


Fig. 1. Density (square), viscosity (circle) and refractive index (triangle) of pure water and water–MTBE mixtures at different concentrations.

negative over the entire range of composition indicating a significant volume contraction on mixing of MTBE with water. On the other hand the positive values of the viscosity deviations suggest that the interaction forces occurring through hydrogen bonding plays an important role in this regard [13]. It is also observed from Table 2 that the adiabatic compressibility (β_S) of the solution shifts to a lower value and the negative magnitude of the deviation in adiabatic compressibility ($\delta\beta_S$) increases with an increase in volume fraction of MTBE solute, which suggests that hydrogen bonding interaction is taking place. A similar conclusion was also drawn for the aqueous binary mixtures of glycol ethers by Dhondge et al. [14]. We have also studied density (ρ), viscosity (η), and refractive index (n_D) of water saturated with MTBE (44.4 mg/ml) from 10 °C to 50 °C as shown in Fig. 2a and Table 3. From the experimental observation, it is also evident that the effect of temperature on viscosity is more pronounced than that on density and refractive index due to the specific hydrogen bonding interactions of MTBE with water molecules. It should be noted that due to a low boiling point of MTBE (55.2 °C) we could not measure the refractive index value of pure MTBE above 40 °C.

The DSC thermograms obtained for water and water–MTBE mixture (44.4 mg/ml) and pure MTBE are shown in Fig. 2b. Upon heating, pure water shows an endotherm at 0 °C which is ascribed to the melting of the ice and is consistent with the reported thermogram in the literature [15]. At MTBE concentration of 44.4 mg/ml, water–MTBE mixture shows a single endotherm at -0.66 °C (Fig. 2b) indicating the formation of extended H-bonding structure among the solvent molecules and the formation of eutectic melt in the solution mixture. In order to infer on the possible formation of any microstructure in the eutectic melt, a prior knowledge of the heat of fusion (ΔH) in the water–MTBE

Table 2

Densities (ρ), excess molar volumes (V^E), viscosities (η), viscosity deviations ($\delta\eta$), refractive index deviations (δn_D), speed of sound (u), adiabatic compressibility (β_S) and deviation in adiabatic compressibility ($\delta\beta_S$) for the mixture of water–MTBE at 20 °C.

[MTBE]/(mg/ml)	$\rho/(\text{g} \cdot \text{cm}^{-3})$	$V^E/(\text{cm}^3 \cdot \text{mol}^{-1})$	$\eta/(\text{cP})$	$\Delta\eta/(\text{cP})$	n_D	δn_D	$u/(\text{m} \cdot \text{s}^{-1})$	$10^{11} \times \beta_S/(\text{N}^{-1} \cdot \text{m}^2)$	$\delta\beta_S/(\text{N}^{-1} \cdot \text{m}^2)$
0.0	0.998204	0.000	1.0066	0.000	1.33301	0.0000	1482.50	45.58	0.000
7.4	0.997289	-0.030	1.0203	0.015	1.33320	7.49e-5	1487.39	45.32	-0.367
14.8	0.996260	-0.057	1.0313	0.027	1.33328	1.00e-4	1493.00	45.03	-0.770
22.2	0.995413	-0.088	1.0403	0.036	1.33351	2.75e-4	1497.68	44.79	-1.123
29.6	0.993632	-0.100	1.0782	0.075	1.33361	3.20e-4	1507.69	44.27	-1.746
37.0	0.992608	-0.126	1.09907	0.089	1.33372	3.76e-4	1513.71	43.97	-2.160
44.4	0.991473	-0.150	1.1280	0.127	1.33391	5.12e-4	1519.79	43.67	-2.570

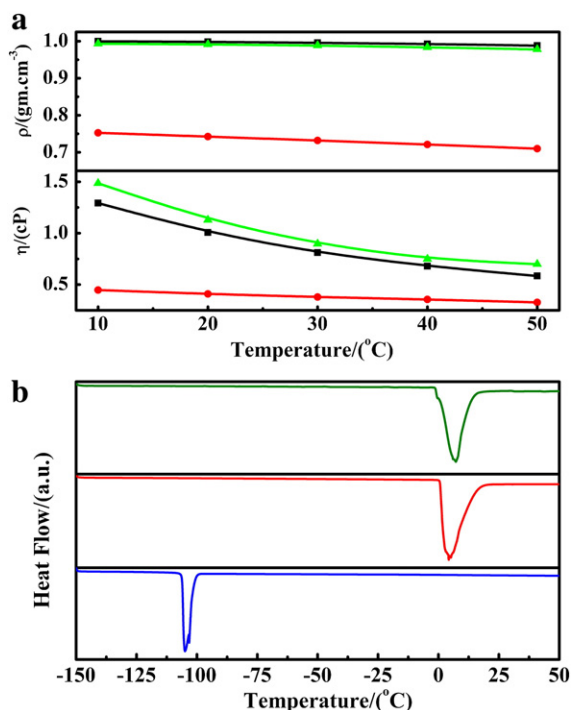


Fig. 2. (a) Temperature dependent density and viscosity of pure water (square), MTBE (circle) and water at highest concentration of MTBE (44.4 mg/ml) (triangle). (b) DSC thermogram of water (middle panel), MTBE (lower panel) and saturated solution of MTBE in water (44.4 mg/ml) (upper panel) using empty vessel as reference.

mixture is very important. The values of enthalpy of fusion determined by the DSC and entropy of fusion for the pure components and for the binary system calculated by the following relation are reported in Table 4.

$$\Delta_f S = \frac{\Delta_f H}{T} \quad (7)$$

where $\Delta_f H$ is the heat of fusion and T is the melting temperature of the compound on absolute scale. The values of the $\Delta_f S$ (Table 4) are found to be positive suggesting that there is an increase in randomness of the system during melting as expected.

If the binary system is assumed to be a mechanical mixture of two components involving no enthalpy of mixing or any type of association in the melt, the heat of fusion could be given by the mixture law [16],

$$(\Delta_f H)_{cal} = x_1 \Delta_f H_1^0 + x_2 \Delta_f H_2^0 \quad (8)$$

where, x_i and $\Delta_f H_i$ are the mole fraction and enthalpy of fusion of the components indicated by the subscripts, respectively. From the calculated values of enthalpy of fusion (Table 4), it can be inferred that they are not simple mechanical mixture of the components. Therefore,

Table 3
Temperature dependent densities (ρ), viscosities (η), refractive indices (n_D) and speed of sound (u) for water–MTBE mixture at a concentration of 44.4 mg/ml.

Sample	Temperature/(°C)	ρ /(g·cm ⁻³)	η /(cP)	n_D	u /(m·s ⁻¹)
Water–MTBE	10	0.993245	1.4849	1.33436	1492.99
	20	0.991473	1.1280	1.33391	1519.79
	30	0.988426	0.8952	1.33205	1537.44
	40	0.983398	0.7482	1.33102	1545.22
	50	0.978066	0.6991	1.32958	1550.82

Table 4
Heat of fusion ($\Delta_f H$) and entropy of fusion data ($\Delta_f S$) of pure water, MTBE and saturated solution of MTBE in water.

Sample	$\Delta_f H$ /(kJ mol ⁻¹)		$\Delta_f S$ /(J mol ⁻¹ K ⁻¹)	
	This work	Literature	This work	Literature
Water	6.11	6.01	22.04	22.00
MTBE	7.57	7.60 [43]	45.32	46.18 [43]
Water–MTBE	4.76	–	17.48	–

the enthalpy of mixing ($\Delta_{mix} H$), which is the difference between the experimental, $(\Delta_f H)_{exp}$ and the calculated values of enthalpy of fusion, $(\Delta_f H)_{cal}$ is given by the equation,

$$\Delta_{mix} H = (\Delta_f H)_{exp} - (\Delta_f H)_{cal} \quad (9)$$

The thermo-chemical studies suggest that the structure of the binary eutectic melt depends on the sign and magnitude of heat of mixing ($\Delta_{mix} H$) [16]. Accordingly, three types of structure are suggested: quasieutectic for which $\Delta_{mix} H > 0$; clustering of molecules in which $\Delta_{mix} H < 0$, and molecular solutions, for which $\Delta_{mix} H = 0$. We have found the value of enthalpy of mixing ($\Delta_{mix} H$) = -1.2 kJ mol⁻¹ for the water–MTBE system suggesting the clustering of molecules in the melt of the binary system.

The direct experimental evidence of the formation of MTBE cluster in water is also revealed in the dynamic light scattering (DLS) experiment as shown in Fig. 3. Fig. 3a depicts the DLS measurement of water–MTBE mixture. The average hydrodynamics diameter (d_H) of the binary mixture at room temperature is about 700 nm (Fig. 3a), which does not change appreciably (within 5% error range) when the MTBE concentration changes in the mixture. Such a high value of d_H thus could be argued due to the formation of aggregate structures in the system and corroborates well with the negative value of the $\Delta_{mix} H$. Similar aggregate structures of water molecules in a hydrophobic solvent (dioxane) were reported recently [17,18]. Fig. 3b shows the persistence of the droplets up to 70 °C, which is much higher than the boiling point of pure MTBE (55.2 °C). The reduced diameter of the aggregates at higher temperature is very much similar with our previous studies on dioxane–water mixture [18,19] and could be due to the shading of water molecules from the hydration layer, as has also been observed for micelles [20] and vesicles [21] at higher temperature. It is important here to note that the solubility of MTBE decreases with an increase in temperature [2]. Therefore there is a possibility to form a super saturated solution at higher temperatures, which could be in non-equilibrium turbid states. However we could not find any such kind of non-equilibrium turbid states. This may be due to the either phase separation of excess MTBE or due to the vaporization of excess MTBE. The single intense peak at 70 °C in our DLS experiment also confirms the absence of any such kind of non-equilibrium turbid states. The formation of micelle-like aggregate [20] of MTBE in the aqueous solution has never been reported in the literature and is a very important consideration for the design of removal strategy of MTBE from the drinking water.

In order to have a better understanding on the interaction mechanism between water and MTBE molecules in the molecular level, we have performed FTIR and Raman measurements. Fig. 4 shows the FTIR absorption spectra of pure MTBE (Fig. 4b) and water saturated with MTBE (Fig. 4a). For pure MTBE the characteristic bands are located at 1021, 1084, 1202, 1232, 1263 and 1365 cm⁻¹. The peaks at 1084 and 1202 cm⁻¹ are assigned to C–O stretching between the oxygen atom and the carbon atom on the methyl group and the tertiary carbon, respectively [9]. The observed vibrational mode at 1232 cm⁻¹ is due to C–C asymmetric stretching between tertiary carbon and methyl carbons opposite to the oxygen atom, because they are strongly coupled and essentially inseparable in nature whereas the peak at 1263 cm⁻¹

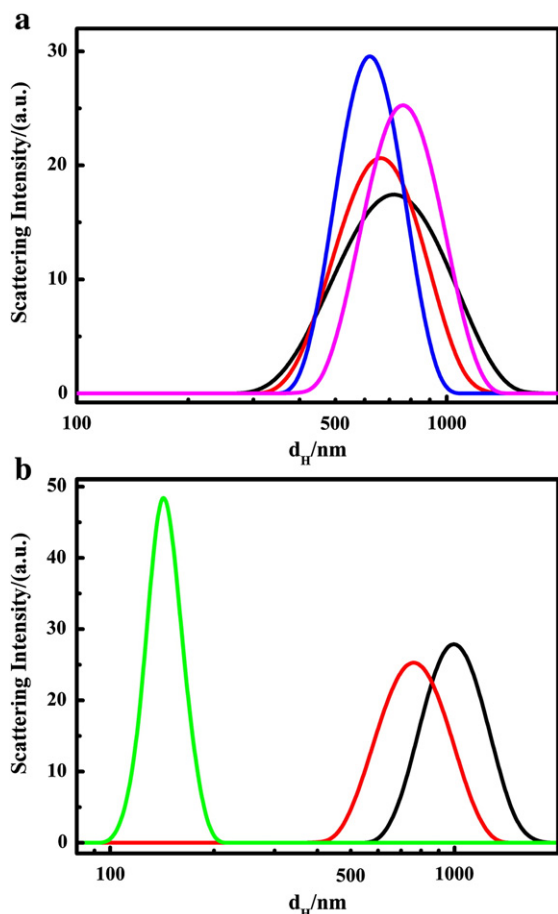


Fig. 3. (a) DLS spectra of water–MTBE mixture at different concentrations of MTBE (black line, 7.4 mg/ml; red line, 14.8 mg/ml; blue line, 29.6 mg/ml; magenta line, 44.4 mg/ml). (b) Temperature dependent DLS spectra of water–MTBE mixture at highest concentration of MTBE (44.4 mg/ml). Black line, 5 °C; red line, 20 °C and green line, 70 °C. (For interpretation of the references to color in this figure, the reader is referred to the web version of this article.)

is assigned to the asymmetric stretching between tertiary carbon and the remaining methyl carbon. The peak at 1021 cm^{-1} is assigned to the CH_3 rocking vibration and 1365 and 1385 cm^{-1} peaks are due to

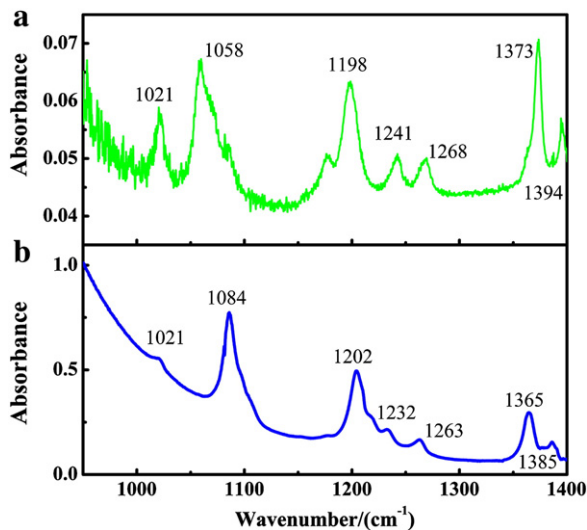


Fig. 4. FTIR spectra of (a) MTBE in water (concentration of MTBE is 44 mg/ml) and (b) pure MTBE. The contribution of water has been subtracted from the FTIR spectra of the solution. (For interpretation of the references to color in this figure, the reader is referred to the web version of this article.)

splitting of the symmetric umbrella deformation. When water molecules are added to MTBE molecules, the hydrogen atom of the water molecules interacts with the oxygen atom of the MTBE molecule through hydrogen bonding. This hydrogen bond tends to weaken the C–O bond of the MTBE molecule, causing an increase in the C–O bond length. The increase of C–O bond length in turn causes a stronger interaction between C–C atoms in $-\text{CCH}_3$ group, which leads to the decrease in the C–C bond length compared to that of the bare MTBE molecule. Therefore, a shift in the vibrational frequencies of MTBE molecules due to the presence of water molecule is expected. Fig. 4b shows the FTIR spectra of MTBE in water. In the presence of water, the peaks of MTBE at 1084 and 1202 cm^{-1} are shifted to lower frequency (red shift) by 26 and 4 cm^{-1} respectively due to the weakening of the C–O bond, and the peaks at 1232 and 1263 cm^{-1} are shifted to a higher frequency (blue shift) by 9 and 5 cm^{-1} due to the strengthening of the C–C bond compared to bare MTBE spectrum. The umbrella bending of $-\text{CH}_3$ is also blue shifted by 9 cm^{-1} whereas the peak due to the rocking vibration of CH_3 at 1021 cm^{-1} is not changed in the presence of water, suggesting that hydrogen bond has little effect on the vibrations that are not associated with the backbone of MTBE molecule.

Fig. 5 shows the Raman spectra of pure MTBE and water–MTBE complex in the frequency range of 50 – 4000 cm^{-1} . In pure MTBE the observed vibrational mode at 725 cm^{-1} is due to the C–C symmetric stretching of tertiary carbon in the *tert*-butyl group [22]. The C–C asymmetric stretching modes of same carbon are observed at 1232 and 1262 cm^{-1} . The peaks at 851 and 1085 cm^{-1} are due to C–O stretching of tertiary carbon and the carbon on methyl group, respectively. The modes that are at 1445 and 1018 cm^{-1} are due to the methyl CH deformation and CH_3 rocking vibration, respectively. The symmetric and asymmetric C–H stretching modes are observed at 2826 , 2915 , 2926 and 2975 cm^{-1} . Two Raman active overtones of the CH_3 “umbrella” deformation splitting are also observed at 2767 and 2708 cm^{-1} . In water–MTBE mixture, similar to our FTIR result, the Raman mode due to C–C asymmetric stretching of tertiary carbon at 1232 and 1262 cm^{-1} are shifted to a higher frequency and modes at 851 and 1085 cm^{-1} , due to C–O asymmetric stretching of tertiary carbon and the carbon on methyl group are red shifted to 845 and 1065 cm^{-1} . Apart from this result, we have found some addition behavior from Raman spectrum. The C–C symmetric stretching of tertiary carbon on methyl group at 725 cm^{-1} is red shifted of about 3 cm^{-1} and the overtones of the CH_3 “umbrella” deformation are blue shifted of about 18 cm^{-1} respectively as shown in Fig. 5b and c. Therefore, the Raman measurements provide a fingerprint of hydrogen bond between hydrogen atom of water molecule and the oxygen atom of the MTBE molecule. Overall FTIR and Raman spectroscopic observations are schematically shown in Scheme 1.

The DLS studies followed by the FTIR and Raman spectroscopic data suggest that the micelle-like MTBE micro-droplets in the aqueous solution are in strong interaction (through hydrogen bonding) with the water molecules. Micelles are well known to solubilize organic matters [23] in the core. Given the fact that MTBE forms a similar structure in water–MTBE mixture, one should expect enhanced solubility of other organic molecules in the mixture. To check the enhanced water solubility of relatively insoluble organic pollutants by dissolved organic matter (DOM), we have investigated the co-solubilization of some model organic matters (pollutants) like anthracene [24,25], naphthalene [26], benzo[α]pyrene [27], and DCM [28] by absorption spectroscopic measurements. It has to be noted here that anthracene, naphthalene and benzo[α]pyrene are the organic pollutants, which are the product of incomplete combustion of the fuel. Fig. 6a (top) shows the relative water solubilities of the pollutant in water and saturated solution of MTBE in water (44.4 mg/ml). A comparison of the results from Fig. 6a indicates that MTBE effectively enhances the water solubility of the organic pollutants in the presence of MTBE. The enhancement of solubility of the hydrophobic solute in the presence of MTBE is also

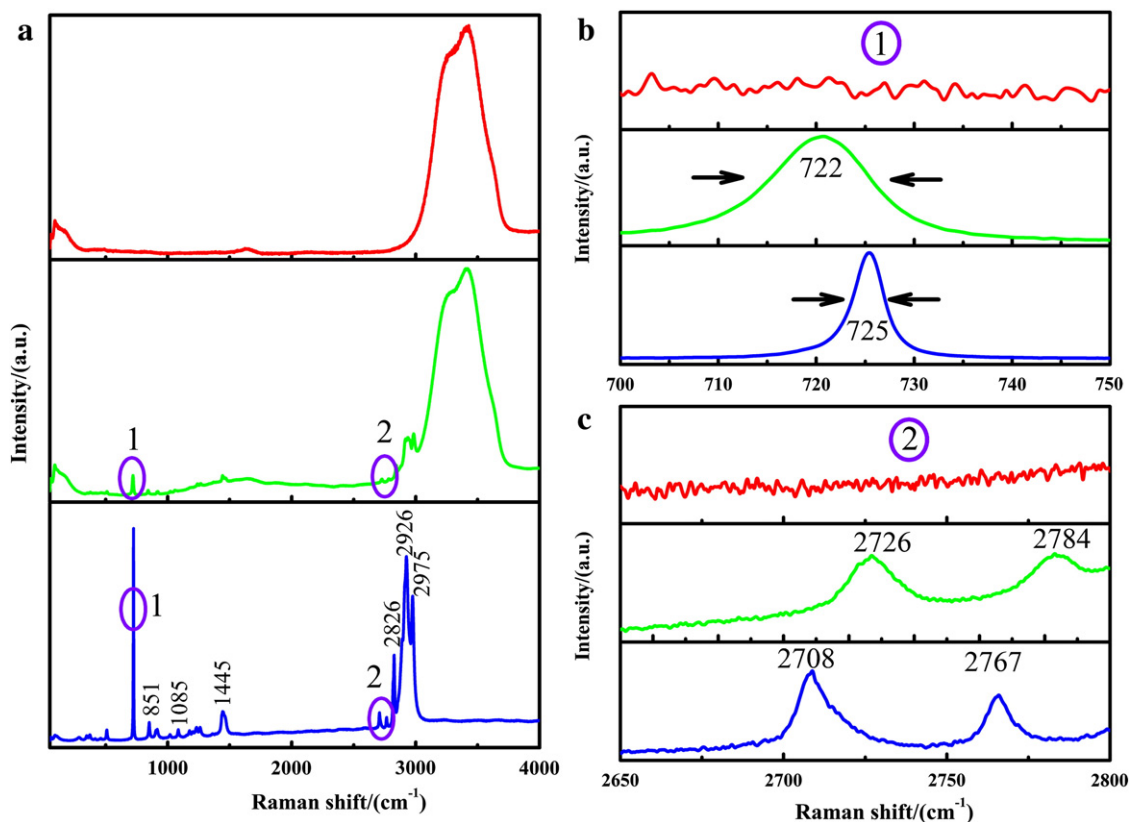
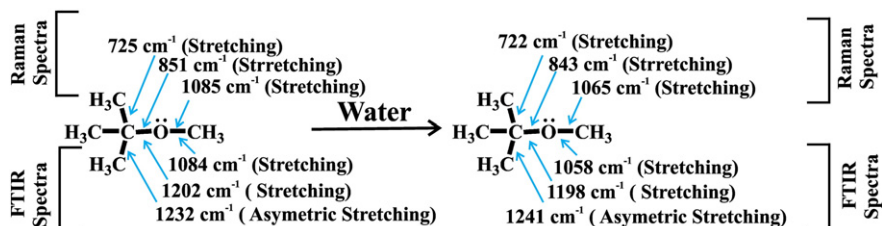


Fig. 5. (a) Raman spectra of water (upper panel), MTBE (lower panel) and water–MTBE mixture (44.4 mg/ml) (middle panel). (b) and (c) are similar spectra of (a) at smaller frequency scale (cm^{-1}) indicated as 1 and 2. (For interpretation of the references to color in this figure, the reader is referred to the web version of this article.)

confirmed by Raman spectroscopy of one of the organic matters that is naphthalene in water–MTBE mixture. Fig. 6b shows the Raman spectrum of solid naphthalene. The intense bands observed at 509, 763, 1380, 1575 and 3053 cm^{-1} are attributed to $-\text{C}-\text{C}-\text{C}-$ bending; radial breathing mode; $\text{C}-\text{C}$ stretching and ring deformation; and in phase $\text{C}=\text{C}$ stretching and out of phase $\text{C}-\text{H}$ stretching, respectively [29]. When naphthalene is dissolved in MTBE, these intense peaks are shifted to of about 2–4 cm^{-1} (right inset of Fig. 6b) showing the interaction of naphthalene with MTBE. However, in water–MTBE mixtures the peaks are not shifted which reveal the presence of naphthalene in the MTBE core. The study thus explores another fatal consequence of MTBE contamination in water, which enhances the solubilization of other hydrophobic organic pollutants in water making contaminated water more polluted.

From the above investigation, it is clear that organic pollutants essentially co-solubilize in the micelle-like hydrophobic core of the MTBE in the aqueous solution. Picosecond-resolved studies on an model organic matter 4-(dicyanomethylene)-2-methyl-6-(*p*-dimethylamino-styryl)-4H-pyran (DCM), which is reported to be mutagenic in nature [28] and well known water-insoluble spectroscopic probe [30–32] is expected to unravel the localization of DCM in the MTBE–water mixture. The emission spectra of DCM in pure MTBE, a relatively polar solvent (methanol) and in the binary mixture are shown in Fig. 7a and b

respectively. In the cluster of the binary mixture solution (Fig. 7b), there are two possible locations of the probe (DCM), e.g., inner hydrophobic core of MTBE cluster or its surface. However, in the hydrophobic core the emission maximum is expected to be similar to that of pure MTBE which is not the case here, rather similar to that on the micellar surface [33]. Another observation is the vivid lengthening of excited state lifetime of DCM in the binary mixture compared to that in pure MTBE. The lifetime of DCM in MTBE is found to be less than 100 ps, which is close to the IRF of our instrument and evidently much shorter than that in the binary mixture (Fig. 7c). The three characteristic fluorescence transients detected at different wavelengths of the DCM emission spectrum in the mixture are shown in Fig. 7c. We have measured the fluorescence lifetime of DCM in the mixture at different wavelengths across the entire emission spectrum and tabulated in Table 5. Fig. 7d–f shows the time-gated fluorescence emission spectrum of DCM in binary mixture. At around $t=0$ ns, DCM shows that emission maximum is around 605 nm and a faster decay profile reveals a distribution of the probe molecules in a non-polar environment. As the time goes, the excited DCM molecules in the non-polar environment come to ground state with their faster lifetime and survive in the relatively polar region (surface of MTBE cluster). In particular, the emission spectrum at 3 ns can be de-convoluted into two distinct spectra



Scheme 1. Schematic representation showing IR and Raman active bands in pure MTBE and in water–MTBE mixture.

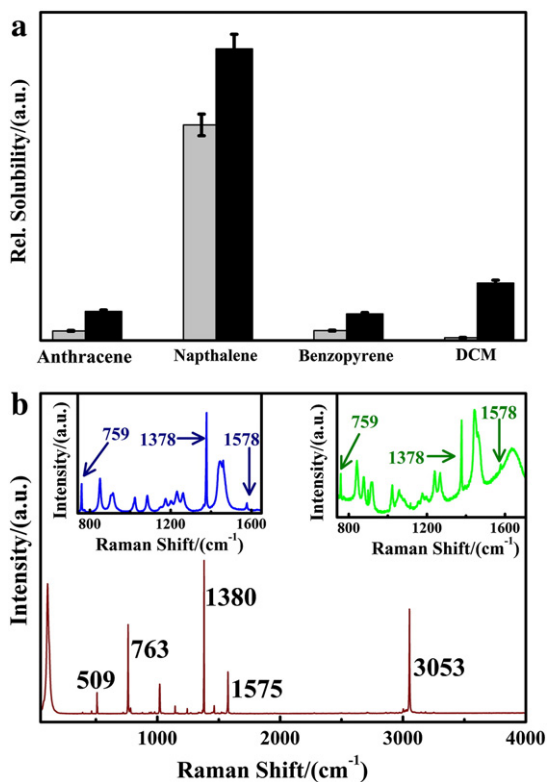


Fig. 6. (a) Relative solubility of model hydrophobic organic pollutant in water (gray box) and water–MTBE mixture (44.4 mg/ml) (black box) with standard error of ~5%. (b) Raman spectrum of solid naphthalene. Inset shows the Raman spectra of naphthalene in pure MTBE (left) and water MTBE mixture (44.4 mg/ml) (right). (For interpretation of the references to color in this figure, the reader is referred to the web version of this article.)

peaking at 605 nm (less-polar) and 655 nm (polar). Eventually, at 8 ns the emission spectrum essentially shows one peak at 655 nm (polar). The picosecond studies thus confirm the localization of the DCM molecules in the heterogeneous environments of micelle like MTBE cluster in water. Our observation also reveals that majority of the DCM population in the ground state (in the absence of light similar to the spectrum at $t=0$) prefer to stay in the non-polar core of the MTBE cluster, which is well described in our recent study [34].

Finally, we study the eco-toxicity of the MTBE–contaminated water on the mortality of a model microorganism (yeast) in light of the mode of action. Microorganisms respond to potentially hazardous organics at various biochemical and physiological levels and their growth rate is diminished to a degree depending on the concentration of the toxic compound(s). However, few studies on MTBE-induced ecotoxicity in vitro can be consulted. Previous ecotoxic effects of MTBE in the model organism *Pseudomonas putida* KT2440 showed that MTBE-concentration of 25.8 mg/ml (293 mM) is sufficient to kill 50% of the cells within 10 min [35]. In the present study the result of the cytotoxicity assay is presented in Fig. 8a. Incubation of yeast cells for 3 h with MTBE at a higher dose level (>29.6 mg/ml) shows a decrease in cell viability compared to control. The results of this study clearly indicate that MTBE metabolism has a relationship with the MTBE concentration and at higher dose levels (29.6 to 44.4 mg/ml) MTBE has direct toxic effects on yeast cells. The metabolic toxicity of MTBE to yeast cell is also evident in the time dependent MTT assay (Fig. 8b), where the MTBE treated yeast cells show reduced production of formazan compared to the control set. In order to find out whether MTBE cytotoxicity has any influence on yeast cell nucleus we stain the MTBE (44.4 mg/ml) treated yeast cell nucleus with DAPI. However, no observable damage of the cell nucleus is noticeable compared to the control experiment (Fig. 8). Although the concentrations used for this experiment is much higher than the concentrations measured in contaminated sites, our studies clearly reveal that metabolic disturbance of yeast by MTBE is a mode of action in the environment.

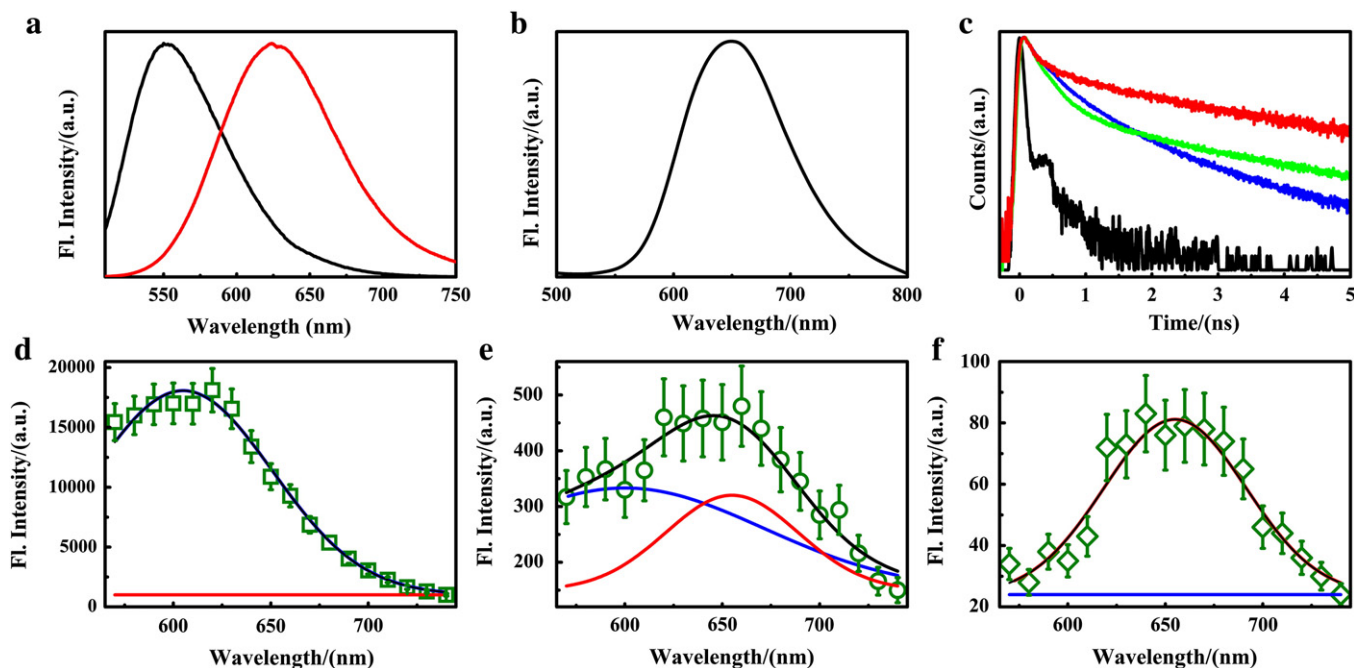


Fig. 7. (a) The steady state emission spectra of DCM in MTBE (black line) and in methanol (red line). (b) Emission spectrum of DCM in water–MTBE mixture (44.4 mg/ml). (c) Fluorescence decay transients of DCM in water–MTBE mixture at different emission wavelengths. Black line, instrument response function (IRF); red line, 740 nm; green line 650 nm and blue line, 570 nm. Time gated fluorescence spectra of DCM in water–MTBE mixture at different time intervals 0 ns, (d); 3 ns (e) and 8 ns (f) with standard error of ~10%. Blue and red lines are the de-convolution spectra showing the presence of DCM in multiple environments. (For interpretation of the references to color in this figure, the reader is referred to the web version of this article.)

Table 5

The fluorescence lifetimes (τ_i) and the relative weight percentage of the time component (a_i) of DCM in saturated solution of MTBE in water with a standard error of ~5%.

Wavelength/(nm)	a_1	τ_1 /(ns)	a_2	τ_2 /(ns)	a_3	τ_3 /(ns)
560	57	0.159	35	0.447	8	1.193
570	57	0.154	33	0.383	10	1.135
580	48	0.135	42	0.307	10	1.109
590	46	0.124	46	0.288	8	1.174
600	30	0.08	62	0.242	8	1.162
610	35	0.0292	59	0.246	6	1.275
620	36	0.094	59	0.239	5	1.437
630	32	0.074	63	0.223	5	1.551
640	31	0.085	64	0.223	5	1.721
650	28	0.07	66	0.214	6	1.809
660	29	0.08	65	0.216	6	1.931
670	30	0.06	63	0.207	7	1.983
680	29	0.066	63	0.207	8	2.046
690	30	0.061	61	0.206	9	2.157
700	25	0.069	66	0.206	9	2.143
710	36	0.086	52	0.218	12	2.209
720	39	0.095	46	0.23	15	2.188
730	67	0.133	18	0.332	15	2.36
740	73	0.133	12	0.644	15	2.806

4. Conclusion

In the present study, we have investigated the interactions between methyl *tert*-butyl ether (MTBE) and water. The thermodynamic quantity like enthalpy of mixing ($\Delta_{mix}H$) indicates the non-ideal mixing of MTBE

with water. The negative value of the excess molar volumes and positive value of viscosity and refractive index deviations support interaction occurring through hydrogen bonding, which is also confirmed from FTIR and Raman spectra. The water solubility study of model hydrophobic organic pollutants in the presence of MTBE shows the enhanced magnitude of water pollution. Finally, the MTBE induced aquatic ecotoxicity shows that metabolic disturbance of yeast by MTBE is a mode of action in the environment and not the morphology change.

Acknowledgment

This work was supported by DST, India (SR/SO/BB-15/2007). S. R. thanks CSIR, India for fellowship. Zaki S. Seddigi wishes to acknowledge the King Abdul Aziz City for Science and Technology (KACST) through the Science & Technology Unit at Umm Al-Qura University for funding support through project No. 10-wat1240-10 as part of the National Science, Technology and Innovation Plan.

References

- [1] C.T. Chiou, R.L. Malcolm, T.I. Brinton, D.E. Kile, *Environmental Science and Technology* 20 (1986) 502–508.
- [2] R.M. Stephenson, *Journal of Chemical & Engineering Data* 37 (1992) 80–95.
- [3] B.G. Bierwagen, A.A. Keller, *Environmental Toxicology and Chemistry* 20 (2001) 1625–1629.
- [4] A. Fischer, M. Müller, J. Klasmeyer, *Chemosphere* 54 (2004) 689–694.
- [5] R.D. Barreto, K.A. Gray, K. Anders, *Water Research* 29 (1995) 1243–1248.
- [6] M.M. Chan, R. Lynch, *Environmental Chemistry Letters* 1 (2003) 157–160.
- [7] A.K. Boulamanti, C.J. Philippopoulos, *Journal of Hazardous Materials* 160 (2008) 83–87.
- [8] T.B. Nielsen, S. Hvidt, S.R. Keiding, C. Petersen, P. Westh, K. Keiding, *Physical Chemistry Chemical Physics* 13 (2011) 1182–1188.
- [9] Z. Li, S. Singh, *Journal of Physical Chemistry A* 112 (2008) 8593–8599.
- [10] L. Morávková, Z. Wagner, J. Linek, *The Journal of Chemical Thermodynamics* 41 (2009) 591–597.
- [11] L. Morávková, Z. Wagner, Z. Sedláková, J. Linek, *The Journal of Chemical Thermodynamics* 42 (2010) 920–925.
- [12] S. Paul, A.K. Panda, *Colloids and Surfaces A: Physicochemical and Engineering Aspects* 404 (2012) 1–11.
- [13] G.-M. Xu, X.-X. Li, Y.-J. Hu, Y.-W. Wang, G.-C. Fan, M. Zhang, *Journal of Chemical & Engineering Data* 55 (2009) 2345–2348.
- [14] S.S. Dhondge, C.P. Pandhurnekar, D.V. Parwate, *Journal of Chemical & Engineering Data* 55 (2010) 3962–3968.
- [15] P. Boonme, K. Krauel, A. Graf, T. Rades, V.B. Junyaprasert, *AAPS PharmSciTech* 7 (2006) E99–E104.
- [16] U.S. Rai, R.N. Rai, *Chemistry of Materials* 11 (1999) 3031–3036.
- [17] C. Yang, W. Li, C. Wu, *The Journal of Physical Chemistry B* 108 (2004) 11866–11870.
- [18] S. Rakshit, R. Saha, P.K. Verma, S.K. Pal, *Photochemistry and Photobiology* 88 (2012) 851–859.
- [19] R.K. Mitra, P.K. Verma, S.K. Pal, *The Journal of Physical Chemistry B* 113 (2009) 4744–4750.
- [20] R.K. Mitra, S.S. Sinha, S.K. Pal, *The Journal of Physical Chemistry B* 111 (2007) 7577–7581.
- [21] R. Saha, P.K. Verma, R.K. Mitra, S.K. Pal, *Colloids and Surfaces B* 88 (2011) 345–353.
- [22] J.B. Cooper, K.L. Wise, W.T. Welch, R.R. Bledsoe, M.B. Sumner, *Applied Spectroscopy* 50 (1996) 917–921.
- [23] D.E. Kile, C.T. Chiou, *Environmental Science and Technology* 23 (1989) 832–838.
- [24] J.T. Oris, J.P. Giesy Jr., *Aquatic Toxicology* 6 (1985) 133–146.
- [25] J.T. Oris, J.P. Giesy, P.M. Allred, D.F. Grant, P.F. Landrum, *Studies in Environmental Science* 25 (1984) 639–658.
- [26] T. Valaes, S.A. Doxiadis, P. Fessas, *Journal of Pediatrics* 63 (1963) 904–915.
- [27] M.F. Denissenko, A. Pao, M.-S. Tang, G.P. Pfeifer, *Science* 274 (1996) 430–432.
- [28] B.J.Y. Wuebbles, J.S. Felton, *Environmental Mutagenesis* 7 (1985) 511–522.
- [29] A. Srivastava, V.B. Singh, *Indian Journal of Pure & Applied Physics* 45 (2007) 714–720.
- [30] H. Zhang, A.M. Jonkman, P. van der Meulen, M. Glasbeek, *Chemical Physics Letters* 224 (1994) 551–556.
- [31] P. van der Meulen, H. Zhang, A.M. Jonkman, M. Glasbeek, *Journal of Physical Chemistry* 100 (1996) 5367–5373.
- [32] S.K. Pal, D. Sukul, D. Mandal, S. Sen, K. Bhattacharyya, *Chemical Physics Letters* 327 (2000) 91–96.
- [33] R. Sarkar, A.K. Shaw, M. Ghosh, S.K. Pal, *Journal of Photochemistry and Photobiology B: Biology* 83 (2006) 213–222.
- [34] S. Rakshit, R. Saha, A. Chakraborty, S.K. Pal, *Langmuir* 29 (2013) 1808–1817.
- [35] M. Krayl, D. Bendorff, N. Loffhagen, W. Babel, *Proteomics* 3 (2003) 1544–1552.
- [36] G.S. Kell, *Journal of Chemical & Engineering Data* 20 (1975) 97–105.
- [37] L. Korson, W. Drost-Hansen, F.J. Millero, *Journal of Physical Chemistry* 73 (1969) 34–39.

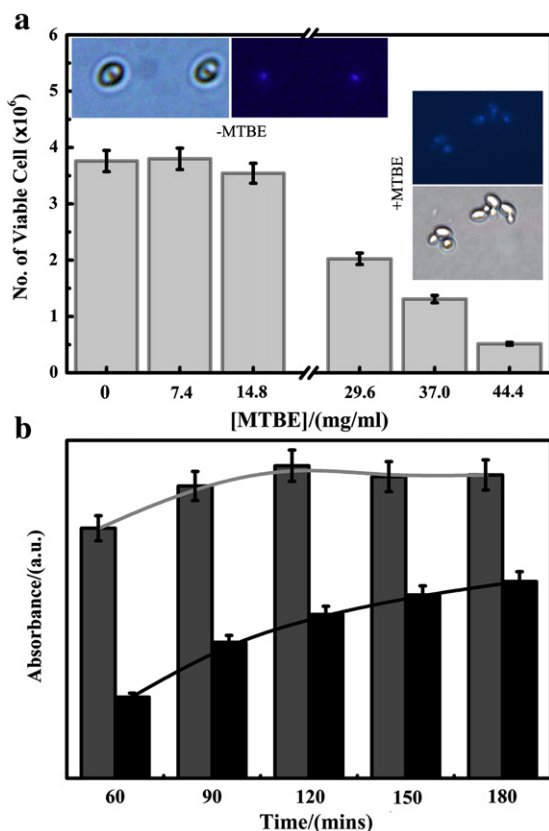


Fig. 8. (a) Effect of MTBE on yeast cell viability at different MTBE concentrations. Inset shows both bright-field and fluorescence micrographic images of DAPI stained yeast cell nucleus upon treatment with MTBE along with the control sets. (b) Time dependent MTT based cytotoxicity assay for the yeast cells in absence (gray box) and presence of MTBE (black box). The standard error of the experiment is about of 5%. (For interpretation of the references to color in this figure, the reader is referred to the web version of this article.)

- [38] A.N. Bashkatov, E.A. Genina, in: V.V. Tuchin (Ed.), *Saratov Fall Meeting 2002: Optical Technologies in Biophysics and Medicine IV*, Spie-Int Soc Optical Engineering, Bellingham, 2002, pp. 393–395.
- [39] R. Gonzalez-Olmos, M. Iglesias, B. Santos, S. Mattedi, *Physics and Chemistry of Liquids* 46 (2008) 223–237.
- [40] D.C. Landaverde-Cortes, A. Estrada-Baltazar, G.A. Iglesias-Silva, K.R. Hall, *Journal of Chemical & Engineering Data* 52 (2007) 1226–1232.
- [41] S. Viswanathan, M. Anand Rao, D.H.L. Prasad, *Journal of Chemical & Engineering Data* 45 (2000) 764–770.
- [42] V. Dumitrescu, *Revista de Chimie* 60 (2009) 293–296.
- [43] E.S. Domalski, E.D. Hearing, *Journal of Physical and Chemical Reference Data* 25 (1996) 1–525.